Supporting Information for

"DNA bending force facilitates Z-DNA formation under physiological salt conditions"

Jaehun Yi[1,‡], Sanghun Yeou[1,‡] and Nam Ki Lee[1,*]

[1] Department of Chemistry, Seoul National University, Seoul, Republic of Korea

[‡] These authors contributed equally

*To whom correspondence should be addressed. E-mail: namkilee@snu.ac.kr

Materials and Methods

DNA sample preparation

We used linear DNA duplexes and D-shaped DNAs. The sequences of the linear DNA duplexes are shown in Figure 1b. The B-Z chimeric linear sample consisted of the CG repeat portion where Z-DNA formation is induced by salt conditions and the random sequence portion where the formation of Z-DNA does not occur.[1] The random linear sample consisted of only a random sequence used as a control. In the case of D-shaped DNAs, the sequence of the double-stranded DNA (dsDNA) portion was the same as that of the B-Z chimeric linear sample, and the single-stranded DNA (ssDNA) string consisted of only thymine to reduce secondary structures (Figure 2c). We prepared various lengths of ring ssDNA by ligating linear ssDNA samples (40, 48, 52, 56 and 80 nucleotides (nt) in Table S1) such that the 5' end of the ssDNA was modified by phosphorylation for ligation. Then, we annealed the ring ssDNA with a complementary 29 nt linear ssDNA (Table S3) to generate D-shaped DNAs (Figure S4). Linear DNAs were prepared by annealing linear ssDNA samples (Table S2) with a complementary 29 nt linear ssDNA (Table S3). The detailed sample preparation method has been described in previous work.[2] We denote a D-shaped DNA nanostructure as BZ29-S23, which means 29 base pairs (bp) of the dsDNA portion and 23 nt of the ssDNA string. To measure single-molecule fluorescence resonance energy transfer (smFRET), ring ssDNA and its partially complementary linear ssDNA were labeled with Cy3 (donor, Amersham) and Cy5 (acceptor, Amersham), respectively. Amine-modified dT, 5' amino modifier C6 and 3' amino modifier were added to label the dyes. All DNA oligomers were purchased from Integrated DNA Technologies.

Alternating-laser excitation confocal microscopy

We investigated the formation of Z-DNA using smFRET measured by alternating-laser excitation confocal microscopy (ALEX). ALEX method and setup have been described in detail in previous work.[2] For ALEX, we used two lasers, one for donor excitation and the other for acceptor excitation, alternatively using acousto-optic modulators (23080-1, Neos Technologies). Two avalanche photodiodes (SPCM AQRH-14, Excelitas) were used to detect each fluorescence emission (Figure S1). DNA samples were diluted to approximately 50 pM using an imaging buffer of 20 mM Tris-HCl (pH 8.0), 100 mM NaCl, 5 % glycerol (v/v), 1 mM MEA, 100 μg/ml BSA, and various concentrations of $Mg(ClO_4)_2$ or $MgCl_2$. Diluted

samples were also incubated for at least 10 minutes. All experiments were performed at room temperature (23 ℃).

Circular dichroism measurements

We measured circular dichroism (CD) spectra to determine the formation of Z-DNA using the circular dichroism spectrometer (Chirascan-plus, Applied Photophysics). We prepared linear and BZ29-S23 samples without dye labeling. Before measurements, the samples were incubated in a buffer with 20 mM Tris-HCl (pH 8.0), 100 mM NaCl, and various concentrations of $Mg(ClO_4)_2$ for at least 30 minutes. The CD measurements were conducted with a sample concentration of at least 4 μM at room temperature. We recorded the CD spectra between 220 nm and 340 nm three times.

2-Aminopurine fluorescence measurements

2-Aminopurine (2-AP) labeled DNA samples were prepared at a final concentration of 5 μM in a buffer with 20 mM Tris-HCl (pH 8.0), 100 mM NaCl, and additional salts (1 M $MgCl_2$ or 2 M $Mg(ClO_4)_2$). The fluorescence emission of 2-AP at 380 nm was measured at room temperature (23 ℃) after the excitation at 320 nm using fluorescence spectrophotometer (Cary Eclipse, Agilent). The fold change in 2-AP emission was calculated as before.[3] The 2-AP labeled ssDNA listed in Table S4 were purchased from Integrated DNA Technologies and annealed with a complementary ssDNA.

Coarse-grained semiflexible loop simulations

A coarse-grained semiflexible loop that consisted of multiple connected nodes was used to simulate the D-shaped DNA (Figure 5a). Five types of nodes were used: a CG node for a CG base pair, an R node for a base pair of random sequences, a Z node for a base pair of Z-DNA, an S node for a nucleotide of the ssDNA string, and a B-Z junction node for a B-Z junction. The interval (a) was set to 0.34 nm for CG and R nodes, 0.37 nm for Z nodes, and 0.7 nm for S and B-Z junction nodes. To equilibrate the loop, a Monte Carlo (MC) simulation with the Metropolis procedure was used.[4] The persistence length (P) was set to 83.7 nm for CG nodes,[5] 50 nm for R nodes, 201 nm for Z nodes,[5] 3 nm for S nodes,[6] and 6 nm for B-Z junction nodes.[7] The bending energy (B) of each node was calculated as $B = P\theta^2/2a$, where θ is the angle between two

tangential vectors of the adjacent nodes. Each MC step of the simulation was carried out as follows: (1) random selection of a single node, (2) random pivotal moving of a selected node, (3) calculating the total bending energy of the semiflexible loop, and (4) acceptance or rejection of the new semiflexible loop based on the Metropolis algorithm. The transformation of a semiflexible loop (SL) into a new semiflexible loop (SL') was accepted with a transition probability $\left(\mathrm{P}\left(SL \rightarrow SL'\right) = \min\left\{1, \exp\left[-\left(\mathrm{E}\left(SL'\right) - \mathrm{E}(SL)\right)/k_B T\right]\right\}\right)$, where $\mathrm{E}(SL)$ is the sum of the bending energies of all nodes in a SL. The loop was equilibrated for 2×10^7 MC steps before recording data during 2×10^7 MC steps. All simulations were performed using homemade scripts (MATLAB 2019b, MathWorks).

From simulations of D-shaped DNAs with various ssDNA string lengths (12, 14, 15, 16, 18, 20, 25, 30 and 40 S nodes), we obtained the end-to-end distance of the dsDNA portion (EED_{dsDNA}), the chord length of the random portion (C_R) and the CG repeat portion (C_{CG}), and the total bending energy of the dsDNA portion (Figures 5b and S13). In the no B-Z transition state, the nodes of the CG repeat portion were set to CG nodes and the nodes of the random portion were set to R nodes. In the B-Z transition with the B-Z junction state, we changed the nodes of the CG repeat portion to Z nodes and the single R node next to the Z node to a B-Z junction node compared to the no B-Z transition state (Figure S13a). The reduced EED_{dsDNA}, C_R, and C_{CG} were obtained by subtracting each distance from its contour length (L_{ds}, L_R, L_{CG}), and the curvature of dsDNA portion (Φ) was calculated using the following equation: $\frac{EED_{dsDNA}}{L_{ds}} = \frac{2}{\Phi}\sin\left(\frac{\Phi}{2}\right)$.

References

1. Ha, S. C.; Lowenhaupt, K.; Rich, A.; Kim, Y.-G.; Kim, K. K., Crystal structure of a junction between B-DNA and Z-DNA reveals two extruded bases. *Nature* **2005,** *437* (7062), 1183-1186.
2. Kim, C.; Lee, O. C.; Kim, J. Y.; Sung, W.; Lee, N. K., Dynamic Release of Bending Stress in Short dsDNA by Formation of a Kink and Forks. *Angew Chem Int Ed Engl* **2015,** *54* (31), 8943-7.
3. Subramani, V. K.; Ravichandran, S.; Bansal, V.; Kim, K. K., Chemical-induced formation of BZ-junction with base extrusion. *Biochemical and Biophysical Research Communications* **2019,** *508* (4), 1215-1220.
4. Metropolis, N.; Rosenbluth, A. W.; Rosenbluth, M. N.; Teller, A. H.; Teller, E., Equation of State Calculations by Fast Computing Machines. *The Journal of Chemical Physics* **1953,** *21* (6), 1087-1092.
5. Thomas, T. J.; Bloomfield, V. A., Chain flexibility and hydrodynamics of the B and Z forms of pory(dG-dC).pory(dG-dC). *Nucleic Acids Research* **1983,** *11* (6), 1919-1930.
6. Murphy, M. C.; Rasnik, I.; Cheng, W.; Lohman, T. M.; Ha, T., Probing Single-Stranded DNA Conformational Flexibility Using Fluorescence Spectroscopy. *Biophysical Journal* **2004,** *86* (4), 2530-2537.
7. Lee, O. c.; Kim, C.; Kim, J.-Y.; Lee, N. K.; Sung, W., Two conformational states in D-shaped DNA: Effects of local denaturation. *Scientific Reports* **2016,** *6* (1), 28239.

DNA sequences

Table S1. Ring ssDNA sequences

Name	Sequences
Ring 40	/5Phos/TGGTTTA/iAmMC6T/CGCGCGCGCGCGCGTTTTTTTTTTTCCTGGAG
Ring 48	/5Phos/TGGTTTA/iAmMC6T/CGCGCGCGCGCGCGTTTTTTTTTTTTTTTTTTTTCCTGGAG
Ring 52	/5Phos/TGGTTTA/iAmMC6T/CGCGCGCGCGCGCGTTTTTTTTTTTTTTTTTTTTTTTTCCTGGAG
Ring 56	/5Phos/TGGTTTA/iAmMC6T/CGCGCGCGCGCGCGTTTTTTTTTTTTTTTTTTTTTTTTTTTCCTGGAG
Ring 80	/5Phos/TGGTTTA/iAmMC6T/CGCGCGCGCGCGCGTTTTTTTTTTTTTTTTTTTTTTTTTTTTTTTTTTTTTTTTTTTCCTGGAG
Ring side 40	/5Phos/TGGTTTATCGCGCGCGCGCGCGTTTTTTTTTTCC/iAmMC6T/GGAG
Ring side 48	/5Phos/TGGTTTATCGCGCGCGCGCGCGTTTTTTTTTTTTTTTTTTTTCC/iAmMC6T/GGAG
Ring side 52	/5Phos/TGGTTTATCGCGCGCGCGCGCGTTTTTTTTTTTTTTTTTTTTTTTCC/iAmMC6T/GGAG
Ring 48 with methylated cytosine	/5Phos/TGGTTTA/iAmMC6T/**C**G**C**G**C**G**C**G**C**G**C**GTTTTTTTTTTTTTTTTTTTCCTGGAG
CG rich ring 52	/5Phos/TGGTTTA/iAmMC6T/CGGTCCAGGCCAGGTTTTTTTTTTTTTTTTTTTTTTTTCCTGGAG

- Cy 3 was labeled at amine-modified dT (/iAmMC6T/). Red color indicates dsDNA portion of D-shaped DNA samples. In the sample with methylated cytosine, bold C indicates methylated cytosine. Phosphorylation (/5Phos/) was added at the 5' end of ssDNA for ligation.

Table S2. Linear ssDNA sequences

Name	Sequences
Linear 29	CCTGGAGTGGTTTA/iAmMC6T/CGCGCGCGCGCGCG
Linear side 29	CC/iAmMC6T/GGAGTGGTTTATCGCGCGCGCGCGCG
Linear 29 with methylated cytosine	CCTGGAGTGGTTTA/iAmMC6T/**C**G**C**G**C**G**C**G**C**G**C**G

CG rich linear 29	CCTGGAGTGGTTTA/iAmMC6T/CGGTCCAGGCCAGG

- Cy 3 was labeled at amine-modified dT (/iAmMC6T/). Red color indicates dsDNA portion of linear DNA. In the sample with methylated cytosine, bold C indicates methylated cytosine.

Table S3. Complementary linear ssDNA sequences (29 nt)

Name	Sequences
Comp 29-5'	/5AmMC6/CGCGCGCGCGCGCGATAAACCACTCCAGG
Comp 29-5' with methylated cytosine	/5AmMC6/CG**C**G**C**G**C**G**C**G**C**GATAAACCACTCCAGG
Comp 29-3'	CGCGCGCGCGCGCGATAAACCACTCCAGG/3AmMO/
Comp 29-Dual	/5AmMC6/CGCGCGCGCGCGCGATAAACCACTCCAGG/3AmMO/
CG rich comp 29-5'	/5AmMC6/CCTGGCCTGGACCGATAAACCACTCCAGG

- Cy5 was labeled at the amine modified 5' end (/5AmMC6/) or the amine modified 3' end (/3AmMO/) except for the comp 29-Dual. In the case of comp 29-Dual, Cy3 and Cy5 were labeled at both ends. The bold C indicates methylated cytosine.

Table S4. 2-AP labeled ssDNA sequences

Name	Sequences
BZ0	CGCGCGCGCGCGCG/i2AmPr/TAAACCACTCCAGG
BZ1	CCTGGAGTGGTTT/i2AmPr/TCGCGCGCGCGCG
BZ7	CGCGCGCGCGCGCGATAAACC/i2AmPr/CTCCAGG

- Adenine base was replaced with 2-AP (/i2AmPr/).

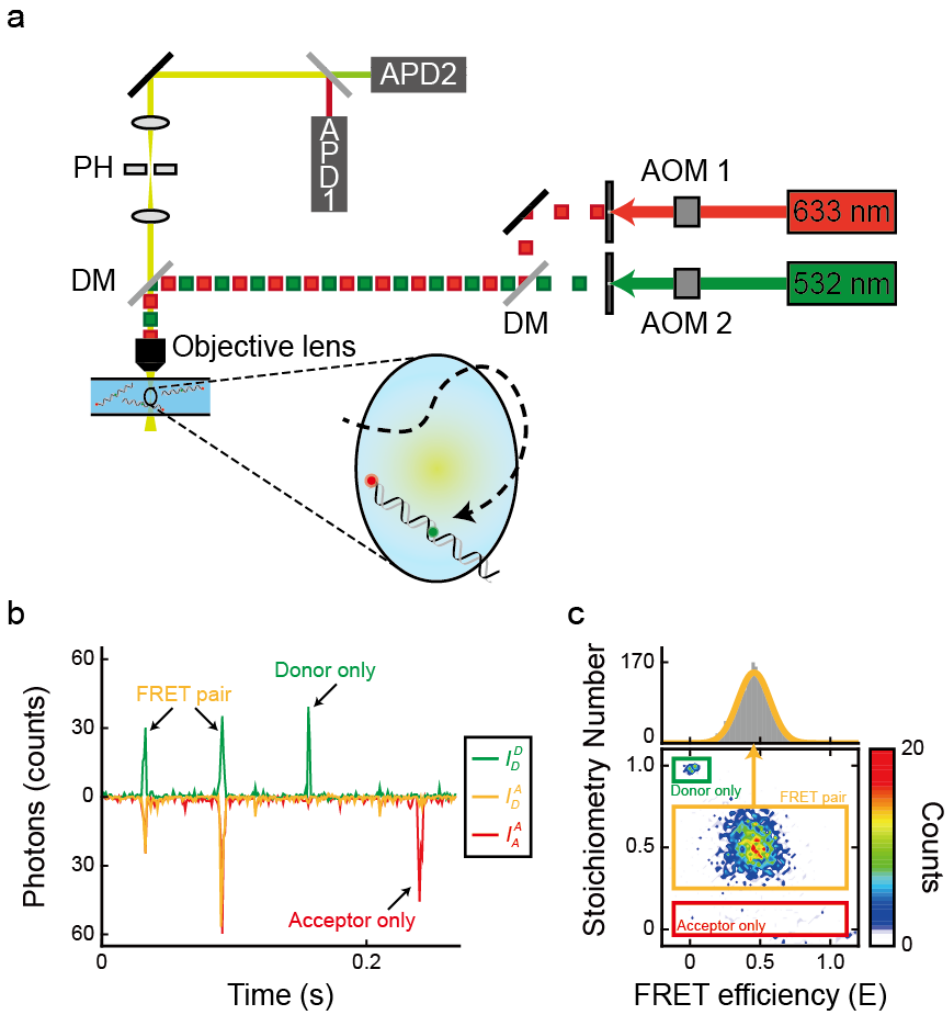

Figure S1. Brief description of the single-molecule alternating laser excitation confocal microscopy (ALEX) setup and measurements. (a) Illustration of the ALEX setup. PH denotes the pinhole, DM denotes the dichroic mirror, APD denotes the avalanche photodiode, and AOM denotes the acoustic optical modulator. The alternating period for the two lasers was 100 μs. (b) Time trace of fluorescent species obtained by the ALEX method. When a single fluorescent molecule passes through the confocal volume, a fluorescent burst is detected. I_D^D denotes the fluorescent signals of donor dyes excited by the donor excitation laser (green), I_D^A denotes the fluorescent signals of acceptor dyes excited by the donor excitation laser (yellow) which refers to the fluorescence resonance energy transfer (FRET) signal, and I_A^A denotes the fluorescent signals

of acceptor dyes excited by the acceptor excitation laser (red). (c) Two-dimensional graph of the FRET efficiency and the stoichiometry obtained by the ALEX method. Using the stoichiometry factor, we classified the samples as donor only, acceptor only and FRET pair species. The green box denotes donor-only labeled species, the yellow box denotes FRET pair labeled species, and the red box denotes acceptor-only labeled species. Only FRET pair-labeled species were selected and analyzed by the one-dimensional FRET efficiency histogram above.

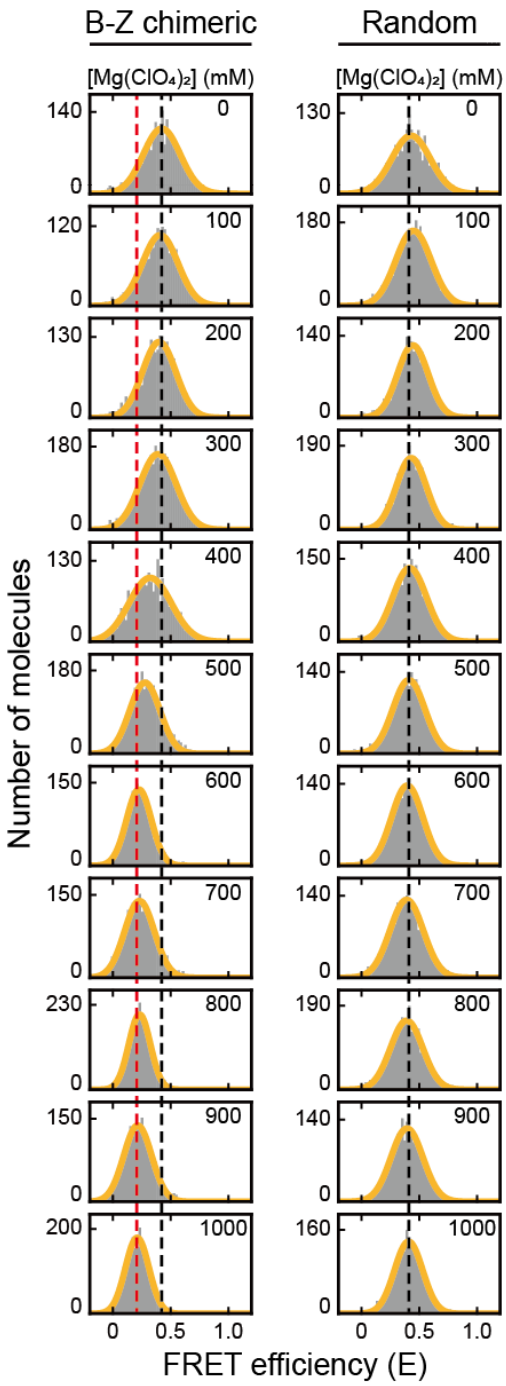

Figure S2. The FRET histograms of the B-Z (chimeric) linear and random linear samples depending on the concentration of magnesium perchlorate ($Mg(ClO_4)_2$). The black dotted lines denote the average FRET efficiency (E) of each sample in the absence of $Mg(ClO_4)_2$. The red dotted line denotes the E of the B-Z

linear sample in the presence of 1000 mM $Mg(ClO_4)_2$. As the concentration of $Mg(ClO_4)_2$ increased, the E of the B-Z linear sample decreased due to the formation of Z-DNA. However, the E of the random linear sample was consistent regardless of $Mg(ClO_4)_2$ concentration. All histograms were fitted to a single Gaussian distribution.

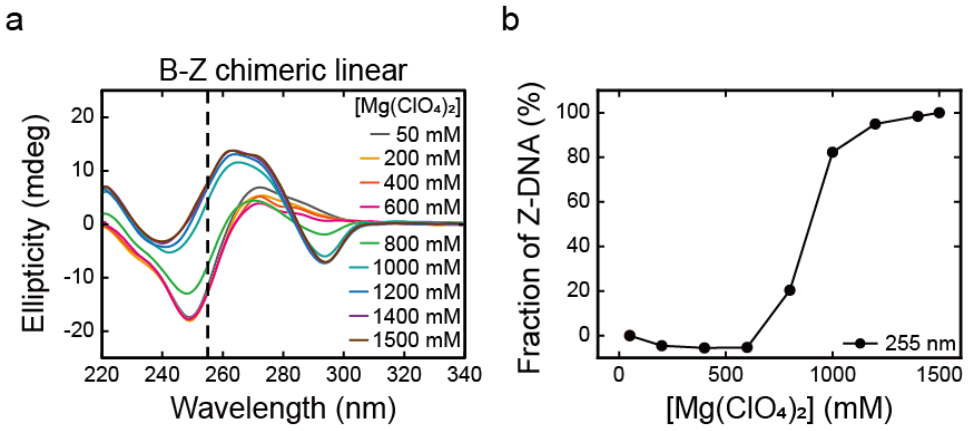

Figure S3. The B-Z transition in the B-Z chimeric linear DNA observed by circular dichroism (CD) measurement. (a) The CD spectra of the B-Z chimeric linear sample at various concentrations of $Mg(ClO_4)_2$. The B-Z chimeric linear sample is the same as that presented in Figure 1b but not labeled with dyes. The black dotted line denotes the wavelength, 255 nm. (b) Fractions of Z-DNA at various concentrations of $Mg(ClO_4)_2$. The data were calculated from Figure S3a. The fraction of Z-DNA was set to 0 % for the lowest salt condition and 100 % for the highest CD signal at 255 nm. The fractions of Z-DNA were obtained from the relative changes in CD signals at 255 nm. The fraction of Z-DNA also indicates the formation of Z-DNA with quantitative dependence on the salt concentration. However, the B-Z transition midpoint from CD measurement is different from that of single-molecule measurement. This is because the remaining B-DNA makes quantitative analysis difficult, and thus, the formation of Z-DNA observed by CD measurement is difficult to be analyzed quantitatively.

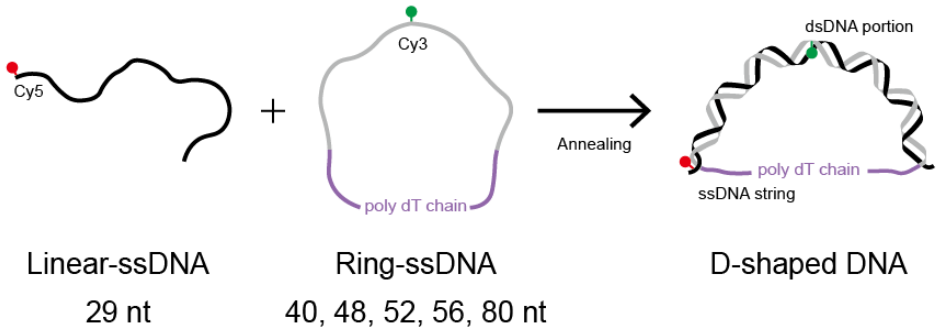

Figure S4. Brief description of the formation of a D-shaped DNA nanostructure. Linear-ssDNA was labeled with Cy 5, and ring-ssDNA samples were labeled with Cy 3. D-shaped DNA is generated by annealing the linear-ssDNA and ring-ssDNA. The stretching force from the ssDNA string (poly T) induces bending of the dsDNA portion.

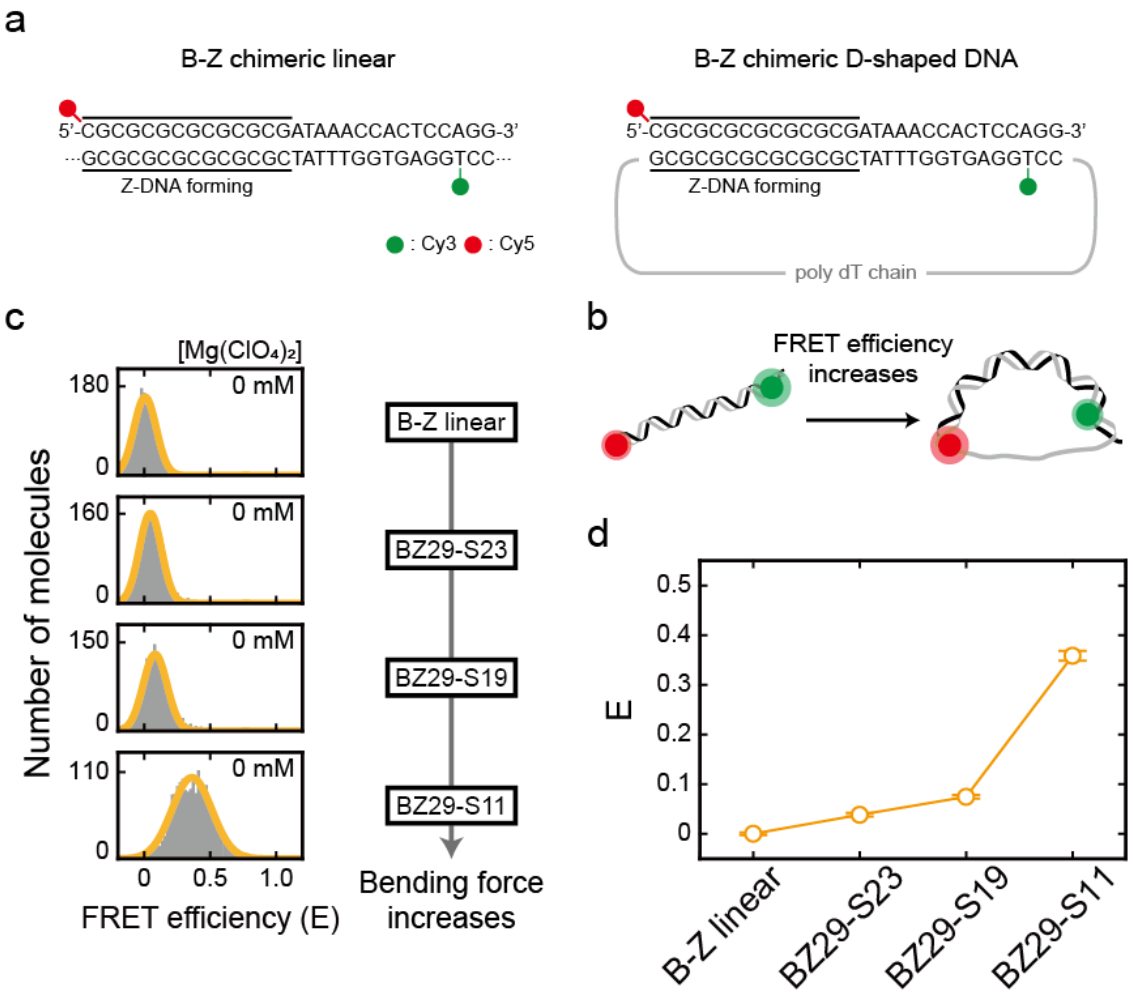

Figure S5. Proving the bending of the dsDNA portion by modulating the ssDNA string length. The effect of the bending force on the dsDNA portion using the B-Z chimeric linear and D-shaped DNAs (BZ29-S23, BZ29-S19 and BZ29-S11) was obtained by the ALEX method. (a) The sequences and labeling positions of the B-Z chimeric linear and D-shaped DNAs. The labeled position of Cy3 was moved from the center to the flank of the dsDNA portion to measure the changes in the end-to-end distance of the dsDNA portion. (b) Schematic illustration for observations of the bending of the dsDNA portion with the FRET efficiency. (c) The FRET histograms of the B-Z (chimeric) linear and D-shaped DNA samples (BZ29-S23, BZ29-S19 and BZ29-S11) at 0 mM $Mg(ClO_4)_2$ obtained by the ALEX method. All histograms were fitted to a single Gaussian distribution. The bending force on the dsDNA portion increased as the ssDNA string length was reduced from 23 nt to 11 nt (BZ29-S23, BZ29-S19, and BZ29-S11) in D-shaped DNAs. Under the low salt condition, 0 mM $Mg(ClO_4)_2$, Z-DNA was not formed. (d) The E values of the B-Z linear and D-shaped

DNAs. As the bending force on the dsDNA portion increased, the curvature of the dsDNA portion increased which was measured by the increase in FRET efficiency E, i.e., shorter distance between the two labeled positions. Error bars were obtained from three independent measurements.

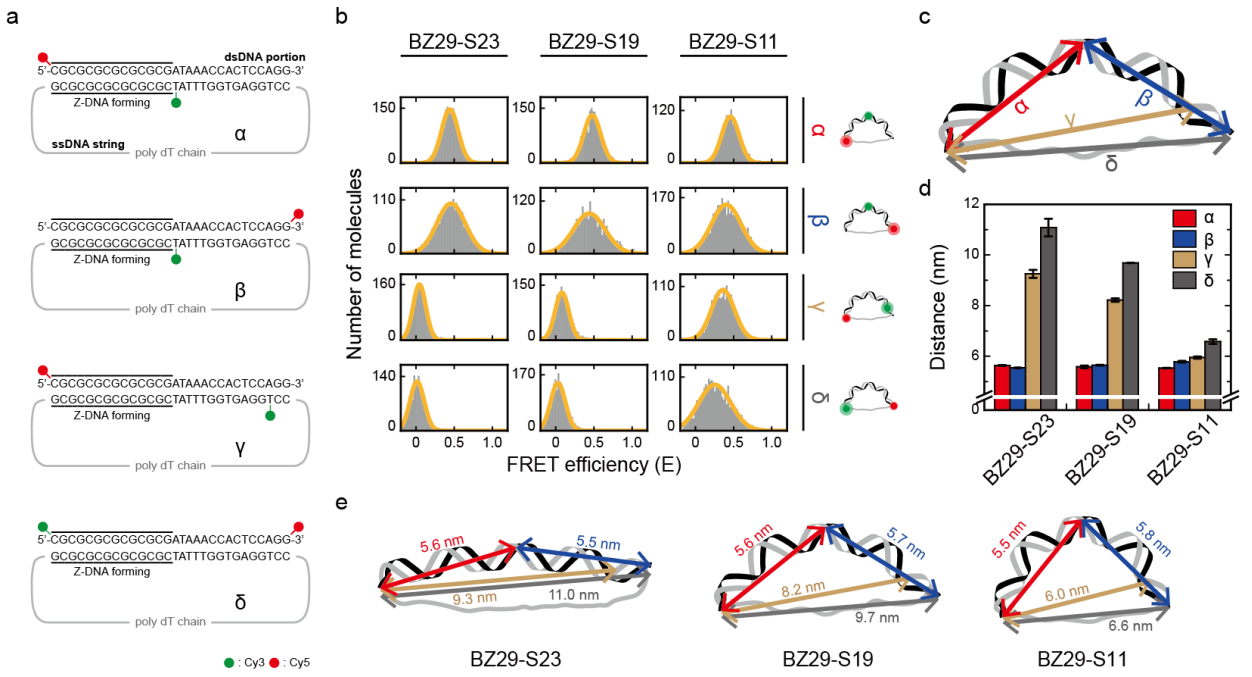

Figure S6. Proving the structures of D-shaped DNAs by measuring multiple distances in each D-shaped DNA (BZ29-S23, BZ29-S19 and BZ29-S11). (a) The sequences and labeling positions of the B-Z chimeric D-shaped DNAs. The sequences of B-Z chimeric D-shaped DNAs were the same as those in Figure 2c, but the FRET dye pairs were labeled at various positions (α, β, γ and δ) of the dsDNA portion in D-shaped DNAs. The distance α and β denote the distances of CG repeats and random portion, respectively. The distance δ is the end-to-end distance of dsDNA portion in a D-shaped DNA and the distance γ is designed to be slightly shorter than the distance δ. (b) The FRET histograms of the B-Z chimeric D-shaped DNA samples (BZ29-S23, BZ29-S19 and BZ29-S11) with various labeling positions at 0 mM $Mg(ClO_4)_2$. Each histogram was fitted to a single Gaussian distribution. The data of the distance δ shown in Figure S5c are presented here again for the purpose of comparison. (c) Schematic illustration of the distances in a D-shaped DNA. (d) The estimated distances of α, β, γ and δ in the D-shaped DNA samples (BZ29-S23, BZ29-S19 and BZ29-S11) from the FRET measurement in (b). As the length of ssDNA string decreased, the distance γ and δ decreased by the bending on dsDNA portion, while the distance α and β did not change, as expected from the structure of D-shaped DNAs. Error bars were obtained from three independent measurements. (e) Schematic illustrations of the distances in each D-shaped DNA. The distance α (5.6 nm), β (5.5 nm), γ (9.3 nm) and δ (11.0 nm) in the BZ29-S23. The distance α (5.6 nm), β (5.7 nm), γ (8.2 nm) and δ (9.7 nm) in the BZ29-S19. The distance α (5.5 nm), β (5.8 nm), γ (6.0 nm) and δ (6.6 nm) in the BZ29-S11.

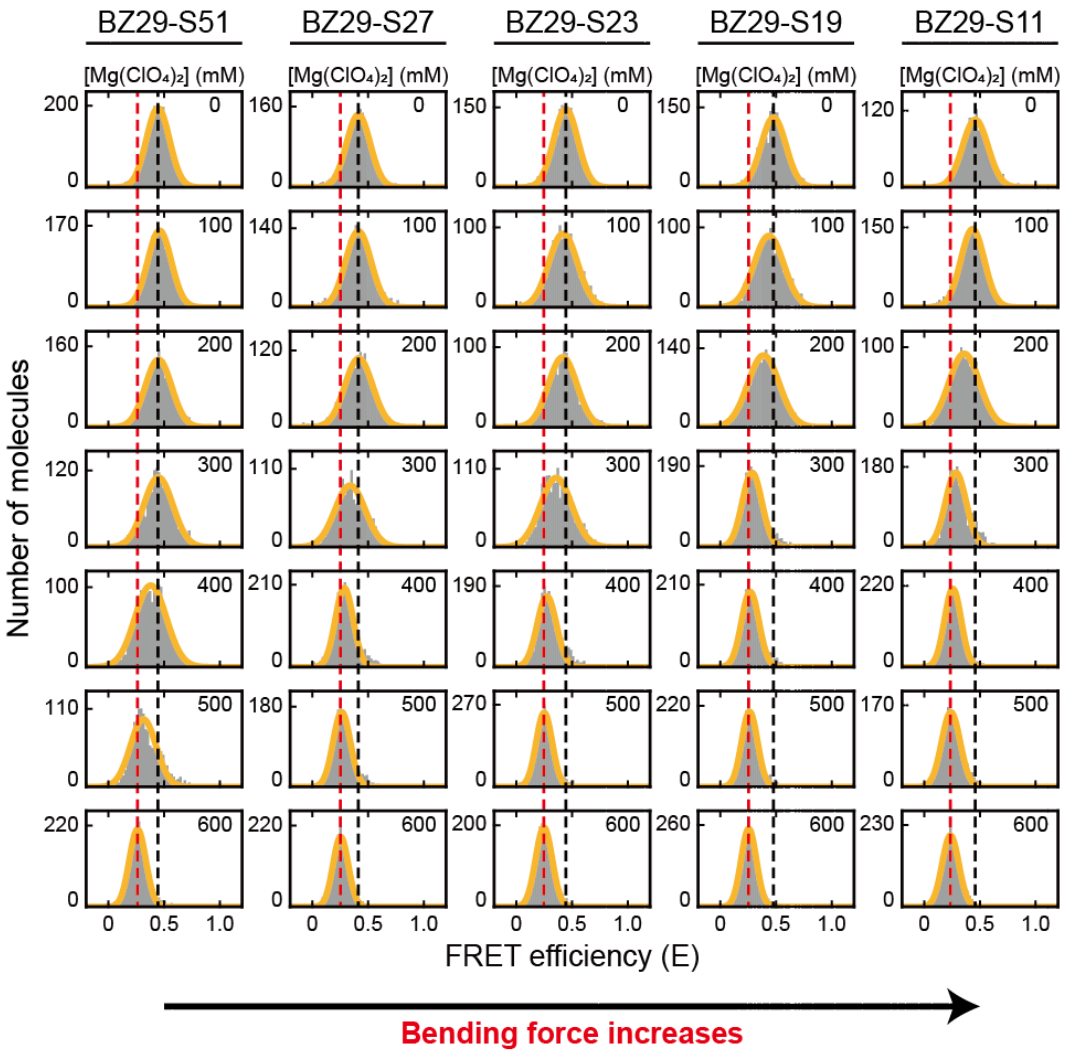

Figure S7. The FRET histograms of D-shaped DNAs (BZ29-S51, BZ29-S27, BZ29-S23, BZ29-S19 and BZ29-S11) depending on the concentration of $Mg(ClO_4)_2$ obtained by the ALEX method. All histograms were fitted to a single Gaussian distribution. The black dotted lines denote the E of each sample in the absence of $Mg(ClO_4)_2$. The red dotted lines denote the E of each sample at 600 mM $Mg(ClO_4)_2$. The decrease in the FRET efficiency (E) occurs at lower salt conditions as the bending force increases.

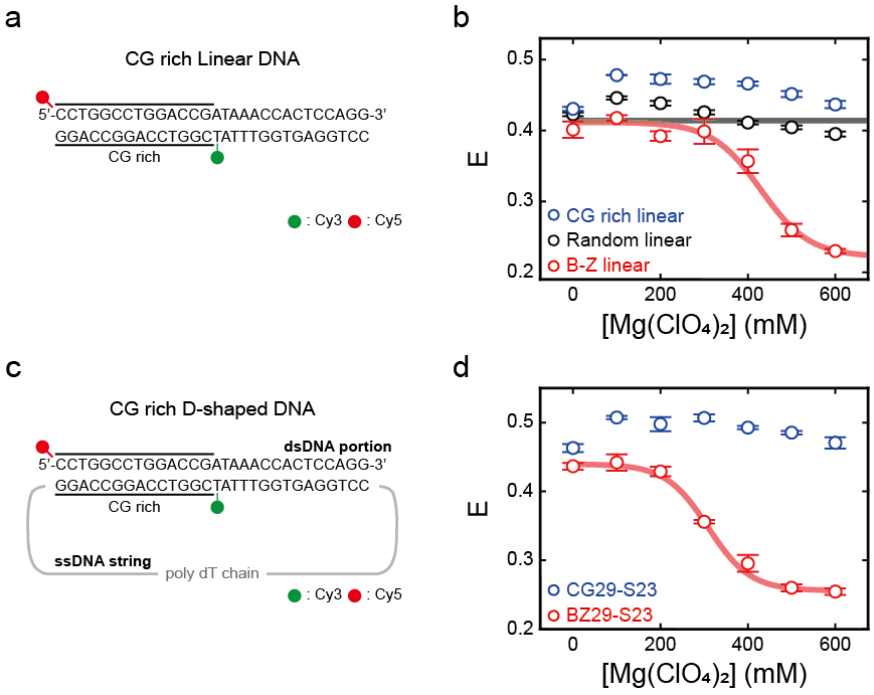

Figure S8. The FRET efficiency E of linear and D-shaped DNA (CG29-S23) with a CG rich region depending on the concentration of $Mg(ClO_4)_2$. (a) DNA sequence of linear DNA with a CG rich region. (b) The FRET efficiency E of linear DNA with a CG rich region (CG rich linear), random region (random linear) and CG repeat (B-Z linear) plotted against the concentration of $Mg(ClO_4)_2$. The data of random linear and B-Z linear are shown in Figure 1e. As the concentration of $Mg(ClO_4)_2$ increased, the E of B-Z linear decreased due to the formation of Z-DNA. However, the E of CG29-S23 did not change which is similar with the E of random linear. Error bars were obtained from three independent measurements. (c) DNA sequence of the D-shaped DNA with a CG rich region. (d) The FRET efficiency E of the D-shaped DNA with a CG rich region (CG23-S23) plotted against the concentration of $Mg(ClO_4)_2$. The BZ29-S23 data are shown in Figure 2e. As the concentration of $Mg(ClO_4)_2$ increased, the E of BZ29-S23 decreased due to the formation of Z-DNA. However, the E of CG29-S23 did not change by the concentration of $Mg(ClO_4)_2$, which indicates that Z-DNA was not formed and the effect of Mg^{2+} concentration on the bending of B-form D-shaped DNA was insignificant.

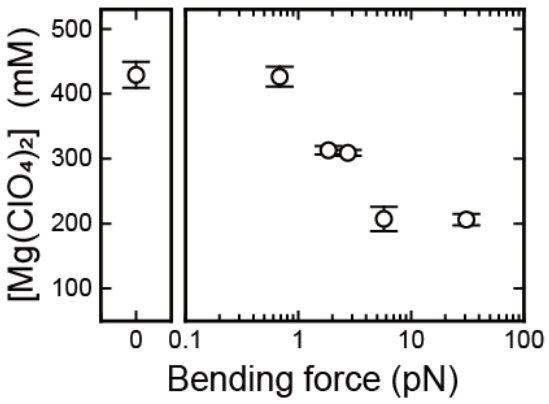

Figure S9. The midpoints of the B-Z transition in each D-shaped DNA depending on the bending force. The bending force of each sample was calculated using a worm-like chain model with the persistence length of 50 nm (dsDNA portion) and 3 nm (ssDNA string) in the equilibrium with the stretching force of the ssDNA string. The calculated bending force was zero piconewtons (pN) in the linear DNA and increased to 30 pN as the length of the ssDNA string decreased in D-shaped DNA nanostructures.

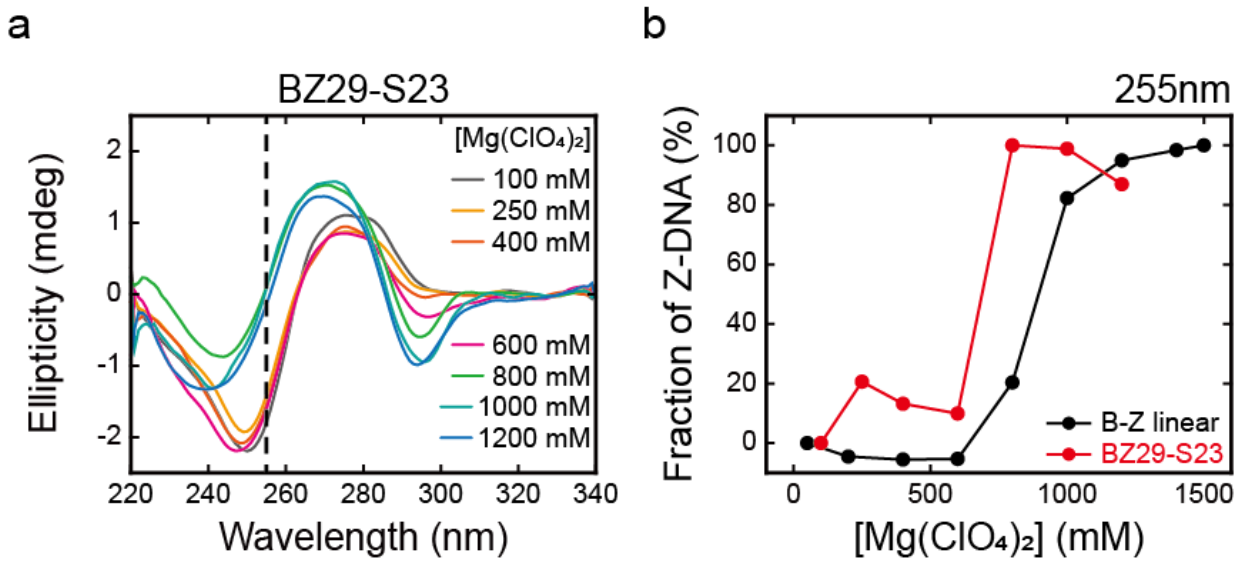

Figure S10. The B-Z transition in the D-shaped DNA (BZ29-S23) observed by CD measurement. (a) The CD spectra of BZ29-S23 at various $Mg(ClO_4)_2$ concentrations. BZ29-S23 sample is the same as presented in Figure 2c but not labeled with dyes. The black dotted line denotes the wavelength, 255 nm. (b) Fractions of Z-DNA in the B-Z linear (no bending force) and BZ29-S23 (with bending force) at various concentrations of $Mg(ClO_4)_2$, which were calculated from the relative changes in the CD signals at 255 nm. The B-Z linear data are shown in Figure S3b. The decrease in the B-Z transition midpoint by the bending force was observed by CD measurement.

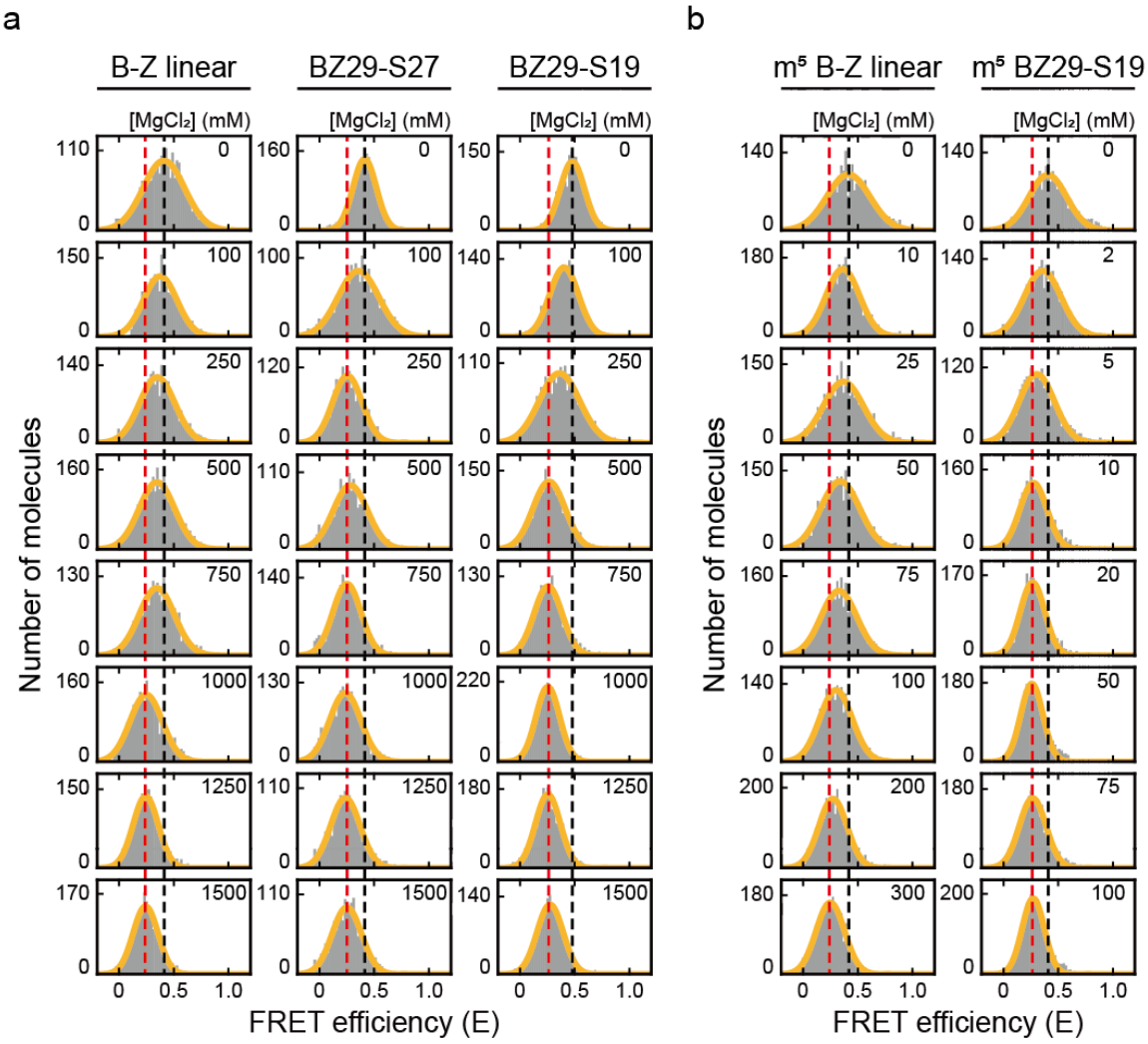

Figure S11. The effects of DNA bending on the B-Z transitions of normal and methylated (indicated as m^5) DNAs by magnesium chloride ($MgCl_2$). (a) The FRET histograms of the B-Z linear and D-shaped DNAs at various concentrations of $MgCl_2$ obtained by the ALEX method. All histograms were fitted to a single Gaussian distribution. The black dotted lines denote the E of each sample in the absence of $MgCl_2$. The red dotted lines denote the E of each sample in the presence of 1500 mM $MgCl_2$. The decrease in E occurs at lower salt conditions as the bending force increases. (b) The FRET histograms of m^5 B-Z linear and m^5 BZ29-S19 depending on the concentration of $MgCl_2$ obtained by the ALEX method. All histograms were fitted to a single Gaussian distribution. The black dotted lines denote the E of each sample in the absence of $MgCl_2$. The red dotted lines denote the E of each sample at the highest concentration of $MgCl_2$ (300 mM for m^5 B-Z linear and 100 mM for m^5 BZ29-S19).

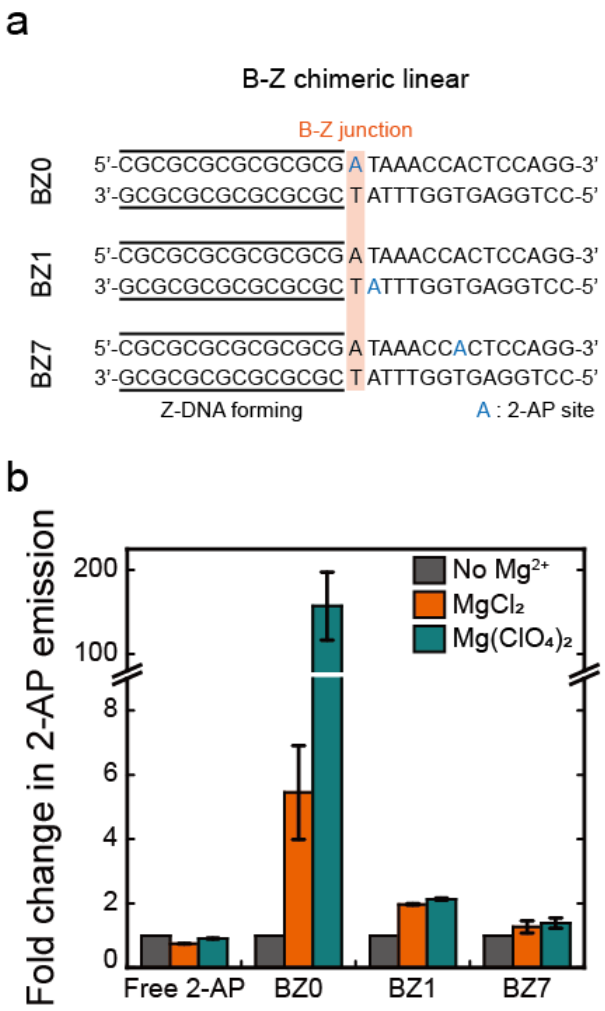

Figure S12. The 2-AP fluorescence measurements depending on 2-AP site with different salt conditions (No Mg^{2+}, 2 M $MgCl_2$ and 1 M $Mg(ClO_4)_2$). (a) Three 2-AP labeled sequences were prepared. BZ0 sample has a 2-AP at the B-Z junction. BZ1 and BZ7 have a 2-AP at one and seven base-pairs away from the B-Z junction, respectively. (b) The fold change in 2-AP emission at 380 nm of free 2-AP base and 2-AP labeled sequences (BZ0, BZ1 and BZ7) depending on salt conditions (No Mg^{2+}, 2 M $MgCl_2$ and 1 M $Mg(ClO_4)_2$). The fold change in 2-AP emission of BZ0 significantly increased with the addition of salt ($MgCl_2$ and $Mg(ClO_4)_2$) compared with 2-AP base only, BZ1, and BZ7 samples. Error bars were obtained from three independent measurements.

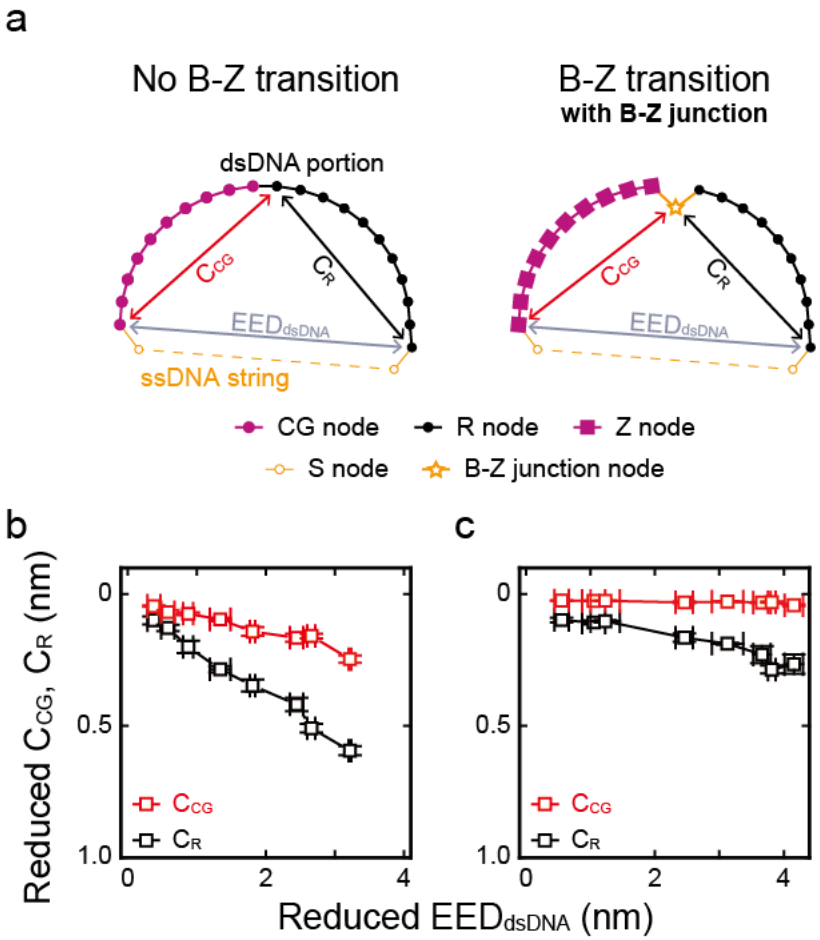

Figure S13. Reduced chord lengths of B- and Z-DNA depending on the reduced end-to-end distance of the dsDNA portion according to two types of the semiflexible loops. (a) Schematic illustration of the simulated semiflexible loops which consisted of a dsDNA portion and a ssDNA string. The end-to-end distance of the dsDNA portion (EED_{dsDNA}), the chord length of the CG repeat portion (C_{CG}) and the random portion (C_R) were obtained using a Monte Carlo simulation. In the no B-Z transition state, the dsDNA portion consists of CG nodes and R nodes. In the B-Z transition with the B-Z junction state, the CG repeat consists of Z nodes and the random portion consists of R nodes, but a B-Z junction node is located between the CG repeat and the random portion. (b) The graph shows that C_{CG} and C_R were reduced as EED_{dsDNA} was reduced in the no B-Z transition state. Error bars were obtained from five independent simulations. (c) The graph shows that C_{CG} and C_R changed little as EED_{dsDNA} was reduced in the B-Z transition with the B-Z junction state. It showed that the B-Z transition decreased the bending of both portions. Error bars were obtained from five independent simulations.